A. W. Reid[1]
Senior Research Fellow
School of Mechanical and Mining Engineering,
The University of Queensland,
St. Lucia, Queensland 4072, Australia
e-mail: anthony.reid@uq.edu.au

P. R. McAree
Professor
School of Mechanical and Mining Engineering,
The University of Queensland,
St. Lucia, Queensland 4072, Australia
e-mail: p.mcaree@uq.edu.au

P. A. Meehan
Associate Professor
School of Mechanical and Mining Engineering,
The University of Queensland,
St. Lucia, Queensland 4072, Australia
e-mail: meehan@uq.edu.au

H. Gurgenci
Professor
School of Mechanical and Mining Engineering,
The University of Queensland,
St. Lucia, Queensland 4072, Australia
e-mail: h.gurgenci@uq.edu.au

Longwall Shearer Cutting Force Estimation

Longwall mining is an underground coal mining method that is widely used. A shearer traverses the coal panel to cut coal that falls to a conveyor. Operation of the longwall can benefit from knowledge of the cutting forces at the coal/shearer interface, particularly in detecting pick failures and to determine when the shearer may be cutting outside of the coal seam. It is not possible to reliably measure the cutting forces directly. This paper develops a method to estimate the cutting forces from indirect measurements that are practical to make. The structure of the estimator is an extended Kalman filter with augmented states whose associated dynamics encode the character of the cutting forces. The methodology is demonstrated using a simulation of a longwall shearer and the results suggest this is a viable approach for estimating the cutting forces. The contributions of the paper are a formulation of the problem that includes: the development of a dynamic model of the longwall shearer that is suitable for forcing input estimation, the identification of practicable measurements that could be made for implementation and, by numerical simulation, verification of the efficacy of the approach. Inter alia*, the paper illustrates the importance of considering the internal model principle of control theory when designing an augmented-state Kalman filter for input estimation.* [DOI: 10.1115/1.4026326]

1 Introduction

The device depicted in Fig. 1 is the shearer of a longwall underground coal mining system. The shearer is responsible for cutting coal from the seam. Once cut, the coal falls onto an armored conveyor and is transported to the surface. This paper presents a methodology for estimating the cutting forces at the *shearer picks* where the cutter heads interact with the coal face.

Direct measurement of the cutting forces acting on an operational shearer has been attempted in the past with only limited success. One approach is to instrument individual picks on the cutter head with strain gauges [1]. This approach suffers from two major drawbacks: the difficulty of maintaining sensors at the coal-cutter interface for any length of time, and that only those picks that are instrumented have their cutting forces measured and the total load on the shearer is unknown. An alternate approach to measure the net cutting forces without instrumenting the rotating cutter head is described in Ref. [2]. In that work, six strain gauges were attached to a single ranging arm and used to resolve the three components of force and three moments acting on the cutter head. Measurements of the hydraulic cylinder pressure, the vertical acceleration of the chassis and tension in the haulage chain were also made. The purpose of the study was to assess the structural design of the ranging arm by applying the measured loads to an associated finite element model, and only required the instrumentation to survive a relatively short period of operation from the commencement of a new coal panel. Sensor reliability was of major concern to the researchers involved.

The current work uses a Kalman filter, based on a system model augmenting the dynamics of the shearer with the dynamics of its forcing inputs, to estimate the cutting forces from indirect measurements. The methodology described is a novel, practical, approach to measuring shearer cutting forces in real-time that overcomes the significant instrumentation challenges of direct force measurement. A result of the paper beyond the specific example of cutting force estimation is to show the benefit of explicitly describing the internal model of the cutting forces in the estimator design. The paper presents several candidate cutting force models designed to represent the mechanics of the force generation process at increasing levels of detail. The models include a constant or step cutting load on the cutter head as well as variations to the cutting load as the cutter head rotates through the seam. The candidate cutting force models are tested in simulation and the results are compared on the basis of cutting force mean and RMS errors.

The structure of the paper is as follows: Sec. 2 discusses the dynamics of the longwall shearer and presents a plant model to be used by the cutting force estimator. In Sec. 3, the internal model principle of control theory [3,4] is discussed in the context of the input estimation problem. Section 4 describes the methodology for input estimation. Section 5 introduces a simulation of a longwall shearer that is used as a testbed for the cutting force estimator. Section 6 reviews the design of shaping filters required to model the unknown cutting force inputs. Section 7 presents the measurements required on the shearer to maintain observability of the cutting force estimator. The approach is tested using the simulation of the longwall shearer in Sec. 8. Finally, conclusions from the work are drawn.

2 Plant Model of the Longwall Shearer

Figure 2 illustrates the shearer plant model for the cutting force estimator. Seven degrees-of-freedom (DOF) are used to describe the five rigid bodies in the 2D shearer model. The first two DOF represent the inertial position of the chassis within the current

[1]Corresponding author.

Contributed by the Dynamic Systems Division of ASME for publication in the Journal of Dynamic Systems, Measurement, and Control. Manuscript received November 21, 2012; final manuscript received December 15, 2013; published online February 19, 2014. Assoc. Editor: Srinivasa M. Salapaka.

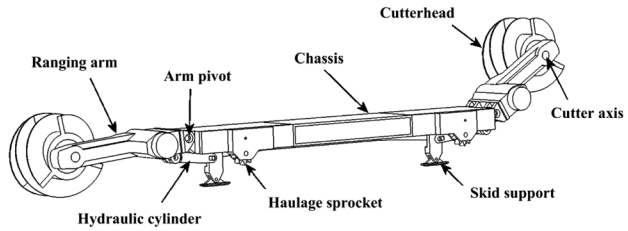

Fig. 1 A dual ranging arm shearer. Two cutter heads (laced with picks) shear coal from the seam and load a conveyor as the shearer moves laterally across the face.

plane of operation. The horizontal location is labeled x, and the vertical location y. The in-plane orientation of the chassis, θ_z, describes the pitching motion as the shearer traverses the face. The chassis-local angles of elevation for the left and right ranging arms are represented by β_l and β_r, respectively. θ_{dl} and θ_{dr} are the orientations of the cutter heads. The plant state vector, $\mathbf{x}_p$, consists of the body velocities in the seven generalized coordinates

$$\mathbf{x}_p = \left[\dot{x}\ \dot{y}\ \dot{\theta}_z\ \left(\dot{\beta}_l - \dot{\theta}_z\right)\ \left(\dot{\beta}_r + \dot{\theta}_z\right)\ \dot{\theta}_{dl}\ \dot{\theta}_{dr}\right]^T \tag{1}$$

A number of the forces acting on the shearer can be modeled and/or measured. These include the haulage forces, F_{hl} and F_{hr}, exerted by the left and right haulage drives via the haulage sprockets and the cutting torques, T_{dl} and T_{dr}, developed by the left and right cutter drives. Also modeled are the moments, M_{rl} and M_{rr}, produced by the left and right hydraulic cylinders about their respective arm pivots to react the cutting loads applied to the ranging arms. The local component of gravity, g, acts through the center of mass of each rigid body.

$$\mathbf{u} = [F_{hl}\ F_{hr}\ T_{dl}\ T_{dr}\ M_{rl}\ M_{rr}\ g]^T \tag{2}$$

Other forces act on the shearer that cannot be measured directly. These are termed *unknown* forces, and will be estimated using the method of state augmentation [5]. The unknown forces include the two orthogonal cutting forces and the cutting torque acting on each cutter head (F_{xl}, F_{yl}, and T_{cl} for the left cutter head and F_{xr}, F_{yr}, and T_{cr} for the right). These are the net cutting loads, representing the cumulative effect of the individual pick forces. Two normal forces, F_{nl} and F_{nr}, are also included that support the shearer chassis vertically. Coulomb friction forces, F_{fl} and F_{fr}, act on the skid supports, opposing shearer translation, and are assumed to be a function of the chassis normal forces.

$$\mathbf{y}_f = [F_{nl}\ F_{nr}\ F_{xl}\ F_{xr}\ F_{yl}\ F_{yr}\ T_{cl}\ T_{cr}]^T \tag{3}$$

$\mathbf{u}$ from Eq. (2) and $\mathbf{y}_f$ from Eq. (3) together form the plant input vector $\mathbf{u}_p$. The shearer plant model takes the form

$$\mathbf{M}\dot{\mathbf{x}}_p = \mathbf{f}_p\left(\mathbf{x}_p, \mathbf{y}_f, \mathbf{u}, \theta_p\right) \tag{4}$$

θ_p is introduced as a set of parameters upon which the dynamic model of the plant depends, including the current orientations of the chassis and the two ranging arms

$$\theta_p = [\theta_z\ \beta_l\ \beta_r] \tag{5}$$

$\mathbf{M}$ is the rigid body inertia matrix, describing the coupling between the various state derivatives

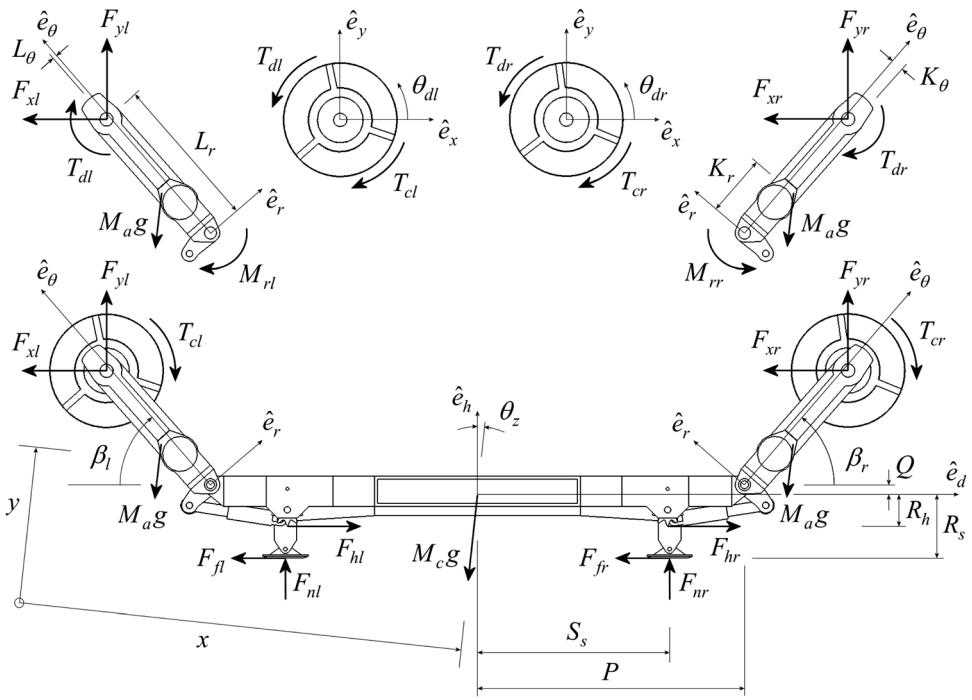

Fig. 2 Planar model of longwall shearer. Five rigid bodies are described by seven degrees of freedom. Generalized coordinates, dimensions and frames of references are shown with thin arrows and external and inertial forces are shown with thick arrows. Model parameters are described in Table 1.

$$\mathbf{M} = \begin{bmatrix} (M_c + 2M_a + 2M_h\cos^2\theta_z) & 2M_h\cos\theta_z\sin\theta_z & (-2M_aQ + 2M_hR_h)\cos\theta_z \\ 2M_h\cos\theta_z\sin\theta_z & (M_c + 2M_a + 2M_h\sin^2\theta_z) & (-2M_aQ + 2M_hR_h)\sin\theta_z \\ (-2M_aQ + 2M_hR_h)\cos\theta_z & (-2M_aQ + 2M_hR_h)\sin\theta_z & (J_c + 2M_a(P^2 + Q^2) + 2M_hR_h^2) \\ M_ay_a(\beta_l - \theta_z) & M_ax_a(\beta_l - \theta_z) & -M_arr_a(\beta_l) \\ -M_ay_a(\beta_r + \theta_z) & M_ax_a(\beta_r + \theta_z) & M_arr_a(\beta_r) \\ 0 & 0 & 0 \\ 0 & 0 & 0 \end{bmatrix}$$

$$\begin{bmatrix} M_ay_a(\beta_l - \theta_z) & -M_ay_a(\beta_r + \theta_z) & 0 & 0 \\ M_ax_a(\beta_l - \theta_z) & M_ax_a(\beta_r + \theta_z) & 0 & 0 \\ -M_arr_a(\beta_l) & M_arr_a(\beta_r) & 0 & 0 \\ \cdots \left(J_a + M_a\left(K_r^2 + K_\theta^2\right)\right) & 0 & 0 & 0 \\ 0 & \left(J_a + M_a\left(K_r^2 + K_\theta^2\right)\right) & 0 & 0 \\ 0 & 0 & J_d & 0 \\ 0 & 0 & 0 & J_d \end{bmatrix} \tag{6}$$

The right side of Eq. (4) can be expressed in the form

$$\mathbf{f}_p\left(\mathbf{x}_p, \mathbf{y}_f, \mathbf{u}, \theta_p\right) = \begin{Bmatrix} f_1 \\ f_2 \\ f_3 \\ f_4 \\ f_5 \\ f_6 \\ f_7 \end{Bmatrix} \tag{7}$$

Where the individual components are defined as follows, and model parameters are described in Table 1.

$$\begin{aligned} f_1 &= -2M_aQ\sin\theta_z\dot{\theta}_z^2 - M_ax_a(\beta_l - \theta_z)\left(\dot{\beta}_l - \dot{\theta}_z\right)^2 + M_ax_a(\beta_r + \theta_z)\left(\dot{\beta}_r + \dot{\theta}_z\right)^2 \\ &\quad + \left(F_{hl} + F_{hr} - F_{fl} - F_{fr} - F_{xl} - F_{xr}\right)\cos\theta_z - \left(F_{nl} + F_{nr} + F_{yl} + F_{yr}\right)\sin\theta_z \\ f_2 &= 2M_aQ\cos\theta_z\dot{\theta}_z^2 + M_ay_a(\beta_l - \theta_z)\left(\dot{\beta}_l - \dot{\theta}_z\right)^2 + M_ay_a(\beta_r + \theta_z)\left(\dot{\beta}_r + \dot{\theta}_z\right)^2 \\ &\quad + \left(F_{hl} + F_{hr} - F_{fl} - F_{fr} - F_{xl} - F_{xr}\right)\sin\theta_z + \left(F_{nl} + F_{nr} + F_{yl} + F_{yr}\right)\cos\theta_z - (M_c + 2M_a)g \\ f_3 &= -M_arr_c(\beta_l)\left(\dot{\beta}_l - \dot{\theta}_z\right)^2 + M_arr_c(\beta_r)\left(\dot{\beta}_r + \dot{\theta}_z\right)^2 + M_{rl} - M_{rr} + R_h(F_{hl} + F_{hr}) \\ &\quad - S_s(F_{nl} - F_{nr}) - R_s\left(F_{fl} + F_{fr}\right) + Q(F_{xl} + F_{xr}) - P\left(F_{yl} - F_{yr}\right) + 2M_aQ\sin\theta_z g \\ f_4 &= -M_arr_c(\beta_l)\dot{\theta}_z^2 + M_{rl} + T_{dl} - F_{xl}y_d(\beta_l) + F_{yl}x_d(\beta_l) - M_ax_a(\beta_l - \theta_z)g \\ f_5 &= -M_arr_c(\beta_r)\dot{\theta}_z^2 + M_{rr} - T_{dr} + F_{xr}y_d(\beta_r) + F_{yr}x_d(\beta_r) - M_ax_a(\beta_r + \theta_z)g \\ f_6 &= T_{dl} - T_{cl} \\ f_7 &= T_{dr} - T_{cr} \end{aligned}$$

The following simplifications have been incorporated in the model, exploiting the symmetry of the shearer. The subscripts l and r are added to the arm orientations in the equations of motion to delineate between the left and right sides. Where global orientations are employed, the + and − signs in the ±correspond to the right and left ranging arms, respectively.

$$x_a(\beta \pm \theta_z) = K_r\cos(\beta \pm \theta_z) + K_\theta\sin(\beta \pm \theta_z) \tag{8}$$

$$y_a(\beta \pm \theta_z) = K_r\sin(\beta \pm \theta_z) - K_\theta\cos(\beta \pm \theta_z) \tag{9}$$

$$x_d(\beta) = L_r\cos(\beta) + L_\theta\sin(\beta) \tag{10}$$

$$y_d(\beta) = L_r\sin(\beta) - L_\theta\cos(\beta) \tag{11}$$

$$rr_a(\beta) = (PK_r - QK_\theta)\cos\beta + (PK_\theta + QK_r)\sin\beta \tag{12}$$

$$rr_c(\beta) = (PK_r - QK_\theta)\sin\beta - (PK_\theta + QK_r)\cos\beta \tag{13}$$

3 The Internal Model Principle

The internal model principle of control theory [3,4] provides guidance on the design of controllers for the dual control

Table 1 Parameters defining the rigid body dynamic model

Symbol	Description
	Chassis parameters
M_c	Mass of shearer chassis.
M_h	Effective mass of a haulage motor and transmission, reflected to the haulage sprocket.
J_c	Mass moment of inertia of shearer chassis about chassis CM.
P	Distance from chassis CM to arm pivots in chassis-local horizontal direction.
Q	Distance from chassis CM to arm pivots in chassis-local vertical direction.
S_s	Distance from chassis CM to skid supports in chassis-local horizontal direction.
R_s	Distance from chassis CM to skid supports in chassis-local vertical direction.
R_h	Distance from chassis CM to haulage sprocket PCD in chassis-local vertical direction.
	Ranging arm parameters
M_a	Mass of the ranging arm including the cutter head.
J_a	Mass moment of inertia of ranging arm including the cutter head mass, about the arm CM.
J_d	Mass moment of inertia of cutter drive reflected to the load.
K_r	Distance from ranging arm pivot to arm CM in arm-local radial direction.
K_θ	Distance from ranging arm pivot to arm CM in arm-local tangential direction.
L_r	Distance from ranging arm pivot to cutting axis in arm-local radial direction.
L_θ	Distance from ranging arm pivot to cutting axis in arm-local tangential direction.

problems of system disturbance compensation and tracking external references. It states that controllers of this type require, as part of their design, a replica or *internal model* of the disturbance or exogenous reference to guarantee zero steady-state error between the controlled variable and its true value. It formalizes the following design methodology: A controller that is required to reject disturbances affecting a system, or that has to track a structured reference signal, must have a duplicate of the disturbance or reference generator in-built, in either the controller or the plant model [3,4].

This theory is consistent with the results of this paper for the problem of observing the input to a dynamic system. The steady-state performance of the cutting force estimator improves as the fidelity of the model describing the dynamics of the unknown inputs increases, and the best performance is achieved when the dynamic structure of the input is duplicated in the augmented-state model of the estimator. This illustrates the importance of considering the internal model principle of control theory when designing an augmented-state Kalman filter for input estimation.

4 Input Estimation Using State Augmentation

The problem of quantifying the forcing inputs to the longwall shearer can be cast in an *optimal estimation* framework. It is well established that a combination of information from both measurements and a system model provides better estimates than those generated from either source alone, provided neither is biased and their uncertainties are quantified. A practical solution that can be readily adapted is the *Kalman filter* [6]. The Kalman filter is applied in a wide range of fields including control, communications, image processing, biomedical science, meteorology, and geology, to estimate the state of dynamic systems. The problem at hand, however, is not to estimate the state of the longwall shearer, but rather its forcing *input*. To achieve this, *state augmentation* is employed whereby the exogenous forcing inputs are modeled as stochastic systems and their states are estimated along with the state of the shearer plant.

Various researchers have applied the approach to estimate external excitation in other applications. Notably, Bayless and Brigham [7] derive the Kalman inverse filter and apply it to the problem of restoring (deconvolving) continuous geophysical signals that have been affected by the dynamics of the seismic measurement process. The discrete-time equivalent followed in Ref. [8]. In Ref. [9], the technique is applied to estimate road roughness. Ray applies the method to the problem of tyre force and road friction estimation [10], as well as to adaptive friction compensation in Ref. [11]. Cui and Ge [12] use the same approach in a combined state-parameter estimation scheme to assist with global positioning system (GPS) navigation in urban canyon environments. Siegrist [13] addresses the problem of estimating tyre forces in off-highway mining trucks, and includes a succinct treatment of the approach.

In a more closely related setting to the rotating cutter head of the longwall shearer, Kim et al. [14] use a Kalman filter disturbance observer to indirectly measure the cutting forces on a commercial horizontal machining center. Here, the model-based estimator is rejected in favor of an artificial neural network (ANN), for its ability to better cope with the complex nonlinear dynamics of the plant[2]. The disadvantage of the ANN, and other data driven estimation methods, is the requirement to provide accurate training data from which the ANN learns the causal relationships between the inputs and the resulting system measurements. An indirect force estimator is desirable because it is not practical to directly measure the forces acting on the longwall shearer to generate a comprehensive training set. For this reason, the model-based approach is more applicable to the problem at hand.

The methodology assumes the plant has known linear (or linearized) dynamics and measurement processes described by the following continuous-time stochastic disturbance and measurement models:

$$\dot{\mathbf{x}}_p(t) = \mathbf{F}_p(t)\mathbf{x}_p(t) + \mathbf{G}_p(t)\mathbf{u}_p(t) + \mathbf{L}_p(t)\mathbf{w}_p(t) \tag{14}$$

$$\mathbf{z}(t) = \mathbf{H}_p(t)\mathbf{x}_p(t) + \mathbf{J}_p(t)\mathbf{u}_p(t) + \mathbf{v}(t) \tag{15}$$

$\mathbf{x}_p(t)$ is the current state of the plant, $\mathbf{u}_p(t)$ is the vector of plant inputs, and $\mathbf{z}(t)$ is the plant measurement vector. The standard definitions apply for the various system and measurement matrices. The noise terms $\mathbf{w}_p(t)$ and $\mathbf{v}(t)$ describe uncertainty in the model of the plant and imprecision in the process of taking measurements. They are assumed to be Gaussian, zero-mean, and white.

The plant input vector contains both known and unknown components. These are represented by $\mathbf{u}(t)$ and $\mathbf{y}_f(t)$, respectively

$$\mathbf{u}_p(t) = \begin{bmatrix} \mathbf{u}(t) \\ \mathbf{y}_f(t) \end{bmatrix} \tag{16}$$

Expressions equivalent to Eqs. (14) and (16) for the longwall shearer were presented as Eqs. (1)–(7) in Sec. 2. The measurement model for the cutting force estimator is introduced in Sec. 7.

The unknown component of the plant input vector cannot be calculated explicitly. It is instead assumed to be a continuous random process, generated by a linear dynamic system perturbed by white noise. The structure of the process model, or *shaping filter*, is determined by any *a priori* knowledge of the input generation mechanism, or from the assumed statistics of $\mathbf{y}_f(t)$. In state space form

$$\dot{\mathbf{x}}_f(t) = \mathbf{F}_f(t)\mathbf{x}_f(t) + \mathbf{L}_f(t)\mathbf{w}_f(t) \tag{17}$$

$$\mathbf{y}_f(t) = \mathbf{H}_f(t)\mathbf{x}_f(t) \tag{18}$$

$\mathbf{x}_f(t)$ is the shaping filter state vector (the *force* states). The noise on these states, $\mathbf{w}_f(t)$, is assumed to be Gaussian, zero-mean and white, implying that the shaping filter encapsulates the complete dynamic structure of the immeasurable inputs.

The *augmented system* state vector is defined

$$\mathbf{x}(t) = \begin{bmatrix} \mathbf{x}_p(t) \\ \mathbf{x}_f(t) \end{bmatrix} \tag{19}$$

The augmented system is driven only by deterministic inputs and is perturbed by Gaussian white noise, satisfying the assumption of

[2]This highlights a need to accurately model the plant dynamics.

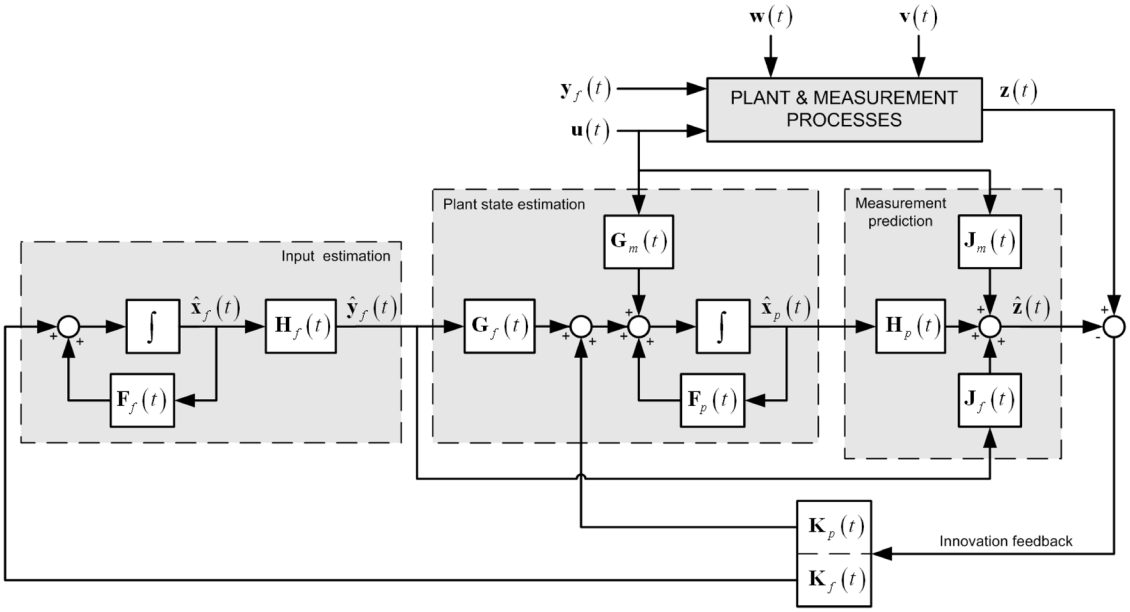

Fig. 3 Kalman filter estimating the state of an augmented system. Note that G_m/G_f and J_m/J_f represent partitions of G_p and J_p, respectively, relating to the known and estimated inputs. The Kalman gain is similarly partitioned.

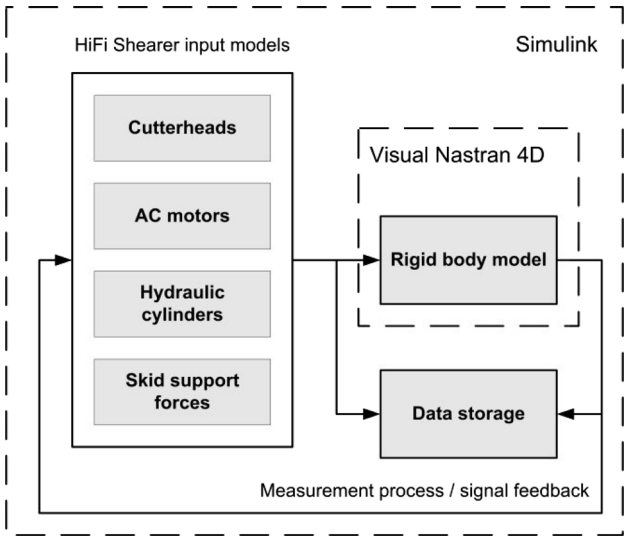

Fig. 4 The structure of the shearer simulation software

the Kalman filter that the plant model is faithful to the real system dynamics. When the augmented model is applied in a Kalman filter (see Ref. [5]), the state estimates include the states of the shaping filters describing the unknown inputs, in addition to the states of the plant. Figure 3 illustrates the structure of the augmented system in a linear continuous-time observer. As the longwall shearer plant model is nonlinear, an extended Kalman filter is applied requiring the linearization of the dynamics about the current state estimate.

5 Simulation of a Longwall Shearer

Figure 4 shows the structure of a longwall shearer simulation that is capable of predicting the forces generated by the shearer in a variety of cutting scenarios. The motivation for the simulation is twofold. First, it acts as the testbed for the shearer cutting force estimator by providing a set of realistic measurements to serve as inputs as well as the fiducial cutting forces against which the force estimates can be compared. Second, it facilitates an investigation into the characteristic structure of the shearer cutting forces in order to duplicate that structure within the design of the shaping filters.

A rigid body assembly incorporating the geometry and inertial properties of the major structures of the shearer is modeled in Visual Nastran 4D and is interfaced with models of the external forcing inputs in the MATLAB Simulink environment. Visual Nastran 4D solves the forward dynamics of the shearer and measurements of the shearer state are made and returned in a feedback loop to the input models. The shearer inputs are divided into four groups:

(1) The fiducial cutting forces and torques experienced by the operational shearer are calculated by a finite-element model of the uncut coal surface around each cutter head. As the cutter drums translate and rotate, the simulation computes the relative motion of each pick through the coal seam and the force that each pick generates [15,16]. The model can be configured for arbitrary pick lacings on the cutter head and for heterogeneous coal seam hardness profiles.
(2) The torques developed by the four AC motors within the shearer are modeled using a vector-based representation [17]. The AC motor models compute the haulage forces required to propel the shearer at the specified haulage speed, and the cutting torques generated to overcome the coal cutting loads. The vector representation is chosen to capture the unsteady motor operation in response to the variable cutting loads experienced by the shearer.
(3) The ranging arm reaction moments are computed from the supporting hydraulic cylinder forces and incorporate a spring model where the cylinder stiffness is derived from the bulk modulus of the hydraulic oil and the internal geometry of the cylinder.
(4) The skid support forces are computed using a spring-damper model to represent the compliance of the supporting structures under the shearer and a Coulomb model for friction.

6 Modeling Shearer Cutting Forces

To ensure that the cutting force estimates contain no steady-state error, the characteristic structure of the true cutting forces must be duplicated in the design of the shaping filters for the augmented Kalman filter. Figure 5 illustrates the horizontal cutting forces (F_{xl}, F_{xr}) and chassis support forces (F_{nl}, F_{nr}) predicted using the shearer simulation in a typical cutting scenario. The horizontal forces are representative of the vertical cutting forces (F_{yl}, F_{yr}) and cutting torques (T_{cl}, T_{cr}). The simulation commences

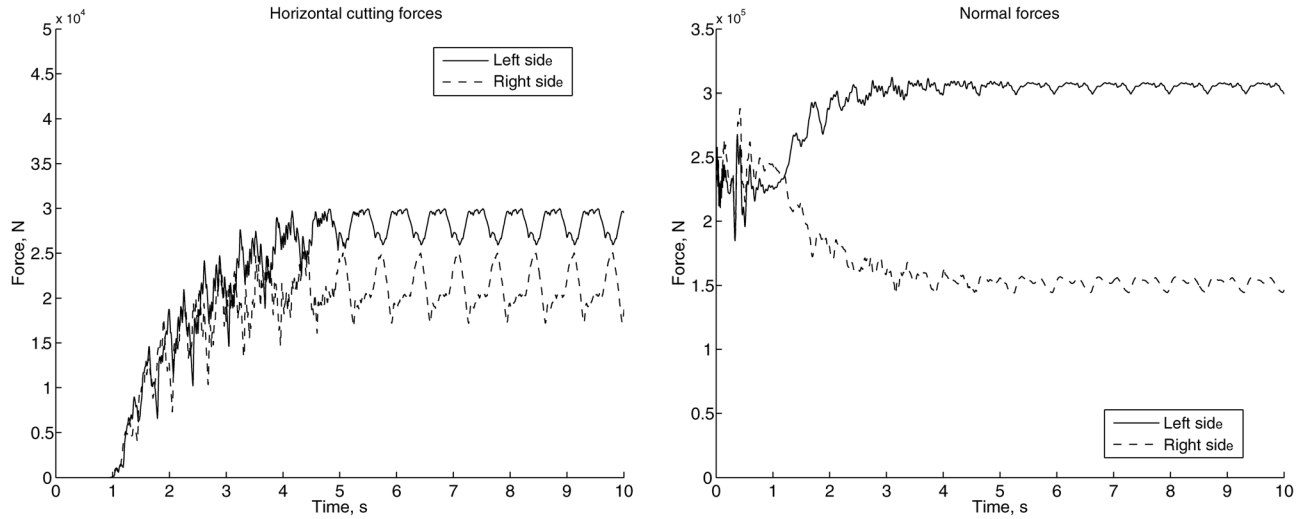

Fig. 5 Horizontal cutting forces (F_{xl}, F_{xr}) and chassis support forces (F_{nl}, F_{nr}) predicted from the shearer plain coal simulation showing the progression of forces from stationary shearer, with cutter heads disengaged from the seam, to steady-state fully-engaged cutting operation. Refer to Fig. 2 for force definition.

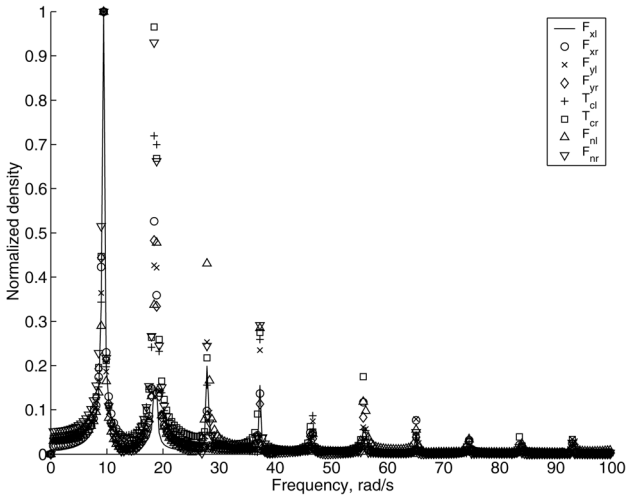

Fig. 6 Spectral density of the unknown shearer inputs. Each of the inputs has a series of harmonics at integer multiples of a base frequency of 9.3 rad/s, *twice* the angular speed of the cutter head. Beyond the seventh harmonic, the density peaks are less than 5% of their maximum values.

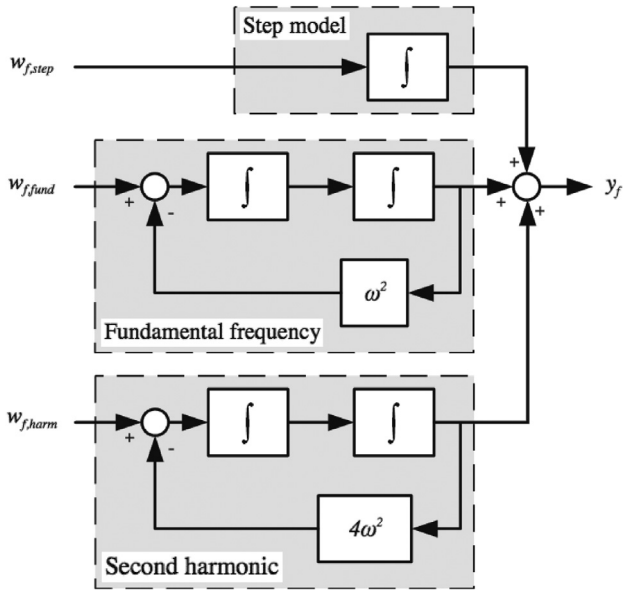

Fig. 7 Shaping filter design combining a step, a sinusoidal input at the fundamental frequency and the second harmonic at twice the fundamental frequency. Additional harmonics (not shown) can be included in the same manner at the summing junction. Uncertainty on the individual shaping filters is represented by independent, Gaussian white noise processes $w_{f,\text{step}}$, $w_{f,\text{fund}}$, and $w_{f,\text{harm}}$ as described in Sec. 4 for application within a Kalman filter framework.

with the shearer stationary and finishes with the shearer cutter heads fully engaged with the coal seam under steady-state operating conditions. The simulation shows that the fiducial cutting forces exhibit a steady-state offset, combined with a significant periodic component resulting from the rotation of the cutter head through the seam. The periodic component of the force deviates as much as 40% from the steady-state mean. By contrast, the chassis support forces do not contain a significant periodic component (varying between 2% and 8% from the steady-state mean).

Two different shaping filter designs are employed for the cutting loads and for the chassis support forces. In accordance with the internal model principle, both shaping filter designs require a *free integrator* representing a step to ensure no steady-state estimate bias. This forms the preliminary shaping filter design for the chassis support forces. The design of the filter for the cutting forces and torques also includes one or more additive sinusoids, at harmonics commencing from twice the cutter head speed[3], that were identified from a spectral analysis of the cutting loads, see Fig. 6. The basic design is illustrated in Fig. 7 for a step and two harmonic frequencies.

7 Required Measurements for Input Estimation

The minimum set of measurements required to estimate the eight unknown forces, and hence make the augmented system completely observable[4], includes direct measurements of the plant model state and a single strain measurement of the net force transfer along the chassis. A larger measurement set is defined for redundancy of information sources. It should be noted that the full set of measurements is practicable and can be made with commercial off-the-shelf sensors.

[3]The pick lacing is repeated twice on the cutter head, resulting in a fundamental frequency of the forcing harmonics that is twice the cutter head angular speed.

[4]Determined by verifying that the observability matrix is full-rank, see [5].

The measurements to be made from the shearer are divided into three groups: state measurements, strain measurements and acceleration measurements. These measurements form the plant measurement model from Eq. (15), and are a non-linear function $\mathbf{h}_p$ of the plant state and inputs

$$\mathbf{z} = [\,\mathbf{z}_x\ \mathbf{z}_\varepsilon\ \mathbf{z}_a\,]^T = \mathbf{h}_p\left(\mathbf{x}_p, \dot{\mathbf{x}}_p, \mathbf{y}_f, \mathbf{u}, \theta_p\right) \tag{20}$$

Seven state measurements are made from the shearer

$$\mathbf{z}_x = \left[\,\dot{d}\ \dot{h}\ \dot{\theta}_z\ \left(\dot{\beta}_l - \dot{\theta}_z\right)\ \left(\dot{\beta}_r + \dot{\theta}_z\right)\ \dot{\theta}_{dl}\quad \dot{\theta}_{dr}\,\right]^T = \mathbf{h}_x\left(\mathbf{x}_p, \theta_p\right) \tag{21}$$

The velocity of the chassis in the chassis-local horizontal direction is $\dot{d}$, and is measured indirectly from motor encoders or tachometers in the haulage drives. The velocity of the chassis in the chassis-local vertical direction is $\dot{h}$. Position measurement using an inertial navigation system has been successfully demonstrated on an operational shearer [18], and could be adapted to measure both chassis translational velocities. The angular velocity measurements, $\dot{\theta}_z, (\dot{\beta}_l - \dot{\theta}_z)$ and $(\dot{\beta}_r + \dot{\theta}_z)$ are assumed to be measured using rate gyroscopes mounted on the three structural bodies. The angular velocities of the left and right cutter heads, $\dot{\theta}_{dl}$ and $\dot{\theta}_{dr}$, are measured using motor encoders or tachometers in the cutter drives. The state measurement model is

$$\mathbf{h}_x\left(\mathbf{x}_p, \theta_p\right) = \begin{cases} \dot{x}\cos\theta_z + \dot{y}\sin\theta_z \\ -\dot{x}\sin\theta_z + \dot{y}\cos\theta_z \\ \dot{\theta}_z \\ \left(\dot{\beta}_l - \dot{\theta}_z\right) \\ \left(\dot{\beta}_r + \dot{\theta}_z\right) \\ \dot{\theta}_{dl} \\ \dot{\theta}_{dr} \end{cases} \tag{22}$$

Three strain measurements are made from the operational shearer

$$\mathbf{z}_\varepsilon = [\,K_{\varepsilon c}\varepsilon_c\ K_{\varepsilon l}\varepsilon_l\ K_{\varepsilon r}\varepsilon_r\,]^T = \mathbf{h}_\varepsilon\left(\mathbf{y}_f, \mathbf{u}, \theta_p\right) \tag{23}$$

The first of these is assumed to be taken from within the main shearer body in such a way as to capture the net force transfer along the chassis. Single strain measurements are also taken from both ranging arms to calculate the net axial forces. The constants $K_{\varepsilon c}, K_{\varepsilon l}$, and $K_{\varepsilon r}$ transform the physical strain measurements (ε_c, ε_l, and ε_r) into equivalent net forces. It is assumed that the strain measurements are not dependent on the cutting torque, gravity or the dynamics of the arms. The strains are modeled as linear functions of known and unknown inputs, with tensile strains defined to be positive

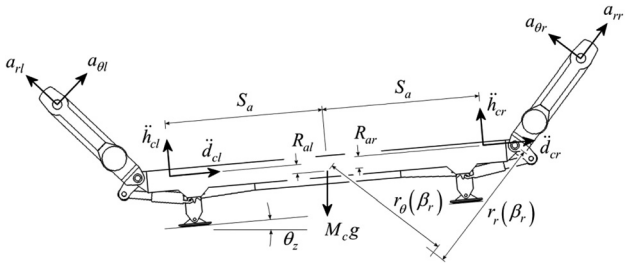

Fig. 8 Acceleration measurements made with sensors mounted in the shearer chassis (symmetrically located S_a from the CM) and ranging arms (at the cutter axis)

$$\mathbf{h}_\varepsilon\left(\mathbf{y}_f, \mathbf{u}, \theta_p\right) = \begin{cases} F_{fl} - F_{fr} - F_{hl} + F_{hr} + F_{xl} - F_{xr} \\ F_{xl}\cos\beta_l + F_{yl}\sin\beta_l \\ -F_{xr}\cos\beta_r + F_{yr}\sin\beta_r \end{cases} \tag{24}$$

Bilinear accelerations are measured from the shearer at four locations, illustrated in Fig. 8, in order to capture both the translational and rotational motions of the chassis and ranging arms

$$\mathbf{z}_a = [\,\ddot{d}_{cl}\ \ddot{h}_{cl}\ \ddot{d}_{cr}\ \ddot{h}_{cr}\ a_{\theta l}\ a_{rl}\ a_{\theta r}\ a_{rr}\,]^T = \mathbf{h}_a\left(\mathbf{x}_p, \dot{\mathbf{x}}_p, \theta_p\right) \tag{25}$$

The first two accelerometers are located at either end of the shearer chassis. From each, two orthogonal acceleration measurements are made in the chassis-local Cartesian coordinate frame. Accelerometers are also mounted at the cutting axes of each ranging arm. These measure orthogonal accelerations in the arm-local polar coordinate frame.

To simplify the acceleration measurement models, the translational acceleration of the chassis CM, transformed to the chassis-local frame of reference, is introduced

$$\ddot{d} = \ddot{x}\cos\theta_z + \ddot{y}\sin\theta_z \tag{26}$$

$$\ddot{h} = -\ddot{x}\sin\theta_z + \ddot{y}\cos\theta_z \tag{27}$$

For the arm acceleration measurement models, a further simplification defines the translational accelerations of the ranging arm pivots (in the chassis-local frame of reference) as functions of the chassis states and state derivatives. The left arm pivot is denoted by subscript *pl* and the right arm pivot by *pr*

$$\ddot{d}_{pl} = \ddot{d} - Q\ddot{\theta}_z + P\dot{\theta}_z^2 \tag{28}$$

$$\ddot{h}_{pl} = \ddot{h} - P\ddot{\theta}_z - Q\dot{\theta}_z^2 \tag{29}$$

$$\ddot{d}_{pr} = \ddot{d} - Q\ddot{\theta}_z - P\dot{\theta}_z^2 \tag{30}$$

$$\ddot{h}_{pr} = \ddot{h} + P\ddot{\theta}_z - Q\dot{\theta}_z^2 \tag{31}$$

The acceleration measurement model is

$$\mathbf{h}_a\left(\mathbf{x}_p, \dot{\mathbf{x}}_p, \theta_p\right) = \begin{cases} \ddot{d} - R_{al}\ddot{\theta}_z + S_a\dot{\theta}_z^2 \\ \ddot{h} - S_a\ddot{\theta}_z - R_{al}\dot{\theta}_z^2 \\ \ddot{d} - R_{ar}\ddot{\theta}_z - S_a\dot{\theta}_z^2 \\ \ddot{h} + S_a\ddot{\theta}_z - R_{ar}\dot{\theta}_z^2 \\ \ddot{d}_{pl}\sin\beta_l + \ddot{h}_{pl}\cos\beta_l + L_r\left(\ddot{\beta}_l - \ddot{\theta}_z\right) + L_\theta\left(\dot{\beta}_l - \dot{\theta}_z\right)^2 \\ -\ddot{d}_{pl}\cos\beta_l + \ddot{h}_{pl}\sin\beta_l + L_\theta\left(\ddot{\beta}_l - \ddot{\theta}_z\right) - L_r\left(\dot{\beta}_l - \dot{\theta}_z\right)^2 \\ -\ddot{d}_{pr}\sin\beta_r + \ddot{h}_{pr}\cos\beta_r + L_r\left(\ddot{\beta}_r + \ddot{\theta}_z\right) + L_\theta\left(\dot{\beta}_r + \dot{\theta}_z\right)^2 \\ \ddot{d}_{pr}\cos\beta_r + \ddot{h}_{pr}\sin\beta_r + L_\theta\left(\ddot{\beta}_r + \ddot{\theta}_z\right) - L_r\left(\dot{\beta}_r + \dot{\theta}_z\right)^2 \end{cases} \tag{32}$$

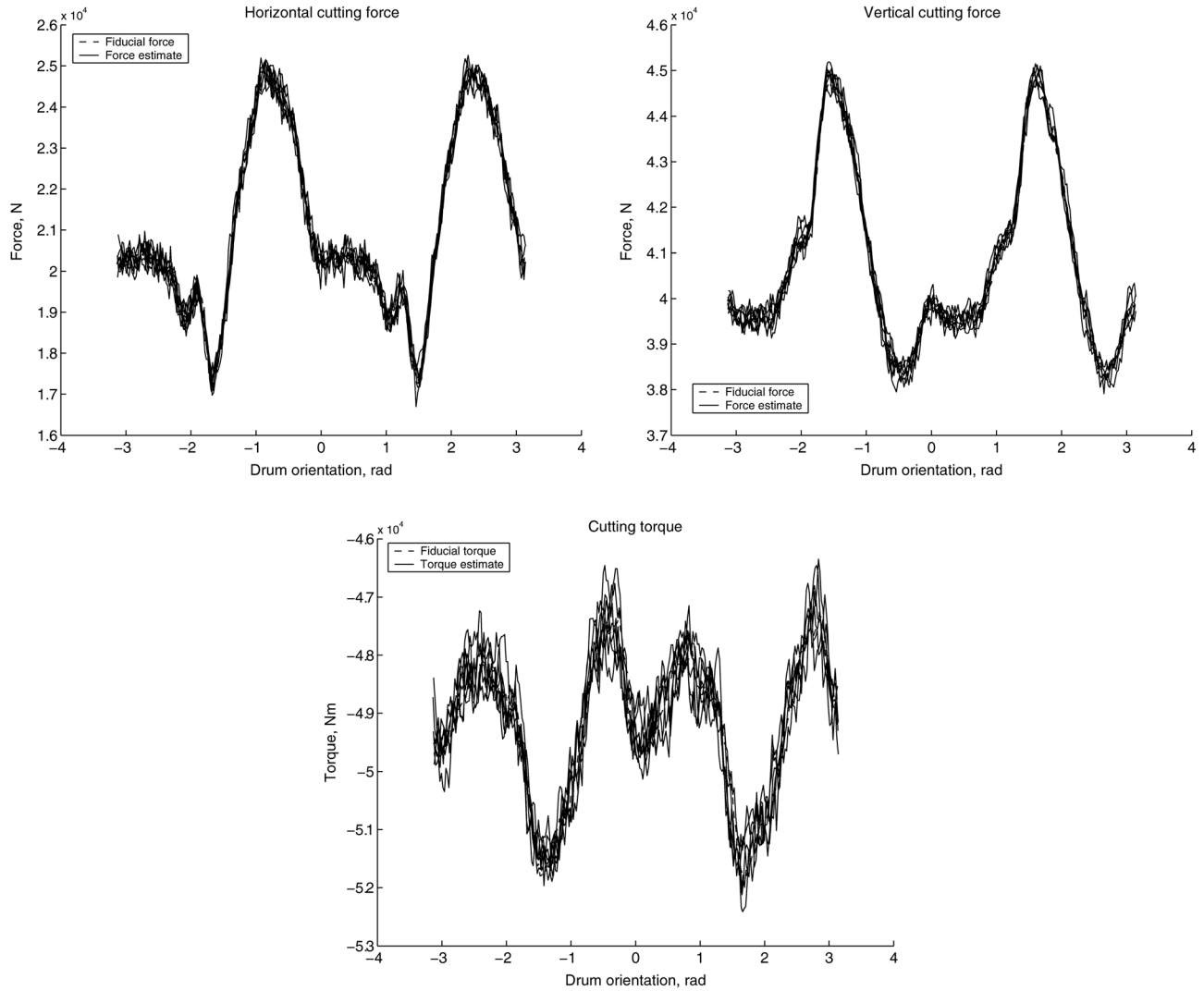

Fig. 9 Steady-state estimates of right side cutting loads versus drum orientation using the offset harmonic 7 filter. Refer to Fig. 2 for force definition. The fiducial forces are indiscernible from the noisy estimates, i.e., the estimates track the fiducial forces well over all drum angles.

The dependence of the acceleration measurements on the state derivative of the plant model, $\dot{\mathbf{x}}_p$, in addition to the plant state, $\mathbf{x}_p$, is addressed by utilizing the plant dynamics directly from Eq. (4).

8 Test Results Using Longwall Shearer Simulation

The simulation of the longwall shearer was used as a testbed for the cutting force estimator. Data recorded from the shearer simulation, and corrupted by additive Gaussian white noise, are treated as measurements made from an operational longwall shearer. The noise covariances were selected to represent that of commercially available, off-the-shelf sensors.

Figure 9 shows the steady-state estimates of the right side cutting loads ($\hat{F}_{xr}, \hat{F}_{yr}$, and $\hat{T}_{cr}$) computed using a shaping filter including a step and sinusoids at seven harmonic frequencies. In each plot, estimates of the cutting loads over multiple drum rotations are plotted against the fiducial loads predicted by the shearer simulation. The performance of the estimator on the right side cutting loads is representative of the estimator performance for the left side.

The fiducial forces are indiscernible from the noisy estimates, i.e., the estimates track the fiducial forces well over all drum angles. Force estimate variability is moderate relative to the underlying signal. The steady-state performance of the estimator is quantified in Table 2 for different shaping filter designs, including: a step filter for all unknown forces, a step and a sinusoid (offset sine filter) for all unknown forces, a step and sinusoids at seven harmonic frequencies (offset harmonic 7 filter) for all unknown forces, and a combination of the offset harmonic 7 filter for the cutting loads and a simplified step filter for the normal forces. Estimator performance is presented in terms of the mean error and RMS error, each as a percentage of the fiducial force mean.

The estimates are all unbiased, resulting from the inclusion of a step model in all shaping filter designs. The best performing filter for the cutting forces and torques, on the basis of highest RMS error, is the *offset harmonic 7 filters and step filters* (F_{nl}, F_{nr}). The highest RMS error is 1.25% of the force mean in $\hat{F}_{xr}$. The *offset harmonic 7 filters* performance is broadly equivalent for the six cutting loads, and the RMS error improves for the chassis support forces, making this the preferred design for the ensemble of unknown shearer inputs.

With only a single frequency sinusoid, the worst RMS error increases to 2.12% in $\hat{T}_{cl}$, and the estimates lag the fiducial forces during rapid changes of force magnitude. An example of the increased RMS error and lag in the estimate of T_{cr} is presented in Fig. 10.

With only a step filter, the worst RMS error is 2.59% in $\hat{T}_{cl}$. These results validate the inclusion of all seven harmonic frequencies in the forcing filters, and show the effect of explicitly

Table 2 Steady-state performance of the force estimator on plain coal using various shaping filter designs

		F_{nl}	F_{nr}	F_{xl}	F_{xr}	F_{yl}	F_{yr}	T_{cl}	T_{cr}
Fiducial forces	$\mu(F)$	305 kN	152 kN	28.4 kN	21.1 kN	−29.3 kN	40.8 kN	38.3 kNm	−49.2 kNm
Step filters	$\mu(\tilde{F})$, %	0.00	0.01	0.00	−0.02	−0.04	0.00	0.04	0.04
	RMSE, %	0.24	0.46	0.84	1.56	1.65	0.97	2.59	1.92
Offset sine filters	$\mu(\tilde{F})$, %	0.00	0.01	0.00	−0.02	−0.04	0.00	0.04	0.05
	RMSE, %	0.25	0.46	0.75	1.50	1.55	0.91	2.12	1.50
Offset harmonic 7 filters	$\mu(\tilde{F})$, %	0.00	0.01	0.00	−0.02	−0.04	0.00	0.04	0.04
	RMSE, %	0.21	0.37	0.59	1.28	1.14	0.54	1.19	0.88
Offset harmonic 7 filters and step filters (F_{nl}, F_{nr})	$\mu(\tilde{F})$, %	0.00	0.01	0.00	−0.02	−0.03	0.00	0.04	0.04
	RMSE, %	0.27	0.49	0.58	1.25	1.13	0.55	1.19	0.88

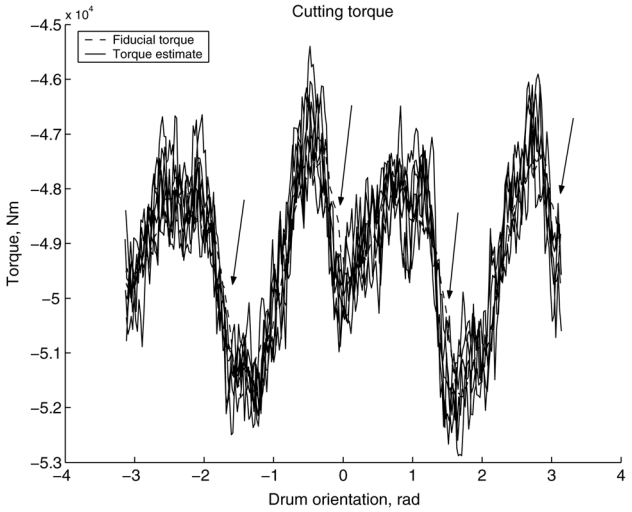

Fig. 10 Steady-state estimates of right side cutting torque versus drum orientation using the offset sine filter. Arrows indicate lagging estimates of T_{cr} due to an incomplete model of the estimated cutting forces and torques.

describing the internal model of estimated exogenous inputs on the RMS errors of the input estimates.

9 Conclusions

This paper presented a methodology for the real-time estimation of longwall shearer cutting forces from indirect, practical measurements. The methodology was tested using simulated measurements from a longwall shearer and the estimator was evaluated with a series of shaping filter designs, incrementally improving the detail with which the dynamic structure of the cutting force inputs are modeled.

The estimator with the lowest RMS error contained the most complete model of the unknown cutting forces, showing the benefit of explicitly describing the internal model of the cutting forces in the estimator design and the importance of considering the internal model principle of control theory when designing an augmented-state Kalman filter for input estimation.

It is noted that although the method proposes measurements that can be made from within the body of the machine, and hence are protected from the mining environment, careful engineering design will be required to ensure the long-term reliability of the sensing hardware.

References

[1] Burchill, R. F., and Waldron, W. D., 1976, "Underground Coal Mine Instrumentation and Test," Final Report, NASA Contract NAS8-31668, George C. Marshall Space Flight Centre, Huntsville, AL.

[2] Takakuwa, T., Wild, G., and Proud, D., 1996, "Measurement of Cutting Forces on the Ranging Arm of a Longwall Shearer and Application of the Results," Proceedings of the Longwall USA International Exhibition and Conference, Pittsburgh, PA, June 4–6, pp. 143–152.

[3] Francis, B. A., and Wonham, W. M., 1976, "The Internal Model Principle of Control Theory," Automatica, **12**(5), pp. 457–465.

[4] Conant, R., and Ashby, W., 1970, "Every Good Regulator of a System Must Be a Model of That System," Int. J. Syst. Sci., **1**(2), pp. 89–97.

[5] Gelb, A., ed., 1974, *Applied Optimal Estimation*, MIT, Cambridge, MA.

[6] Kalman, R. E., 1960, "A New Approach to Linear Filtering and Prediction Problems," ASME J. Basic Eng., **82**, pp. 35–45.

[7] Bayless, J. W., and Brigham, E. O., 1970, "Application of the Kalman Filter to Continuous Signal Restoration," Geophys., **35**(1), pp. 2–23.

[8] Crump, N. D., 1974, "A Kalman Filter Approach to the Deconvolution of Seismic Signals," Geophys., **39**(1), pp. 1–13.

[9] Jeong, W., Yoshida, K., Kobayashi, H., and Oda, K., 1990, "State Estimation of Road Surface and Vehicle System Using a Kalman Filter," JSME Int. J. Ser. III—Vib. Control Eng., **33**(4), pp. 528–534.

[10] Ray, L. R., 1997, "Nonlinear Tire Force Estimation and Road Friction Identification: Simulation and Experiments," Automatica, **33**(10), pp. 1819–1833.

[11] Ray, L. R., Ramasubramanian, A., and Townsend, J., 2001, "Adaptive Friction Compensation Using Extended Kalman-Bucy Filter Friction Estimation," Control Eng. Pract., **9**, pp. 169–179.

[12] Cui, Y., and Ge, S., 2001, "Autonomous Vehicle Positioning With GPS in Urban Canyon Environments," Proceedings of the IEEE International Conference on Robotics and Automation (ICRA), Vol. 2, Seoul, Korea, May 21–26, pp. 1105–1110.

[13] Siegrist, P., 2004, "A Methodology for Monitoring Tyre-Forces on Off-Highway Mining Trucks," Ph.D. thesis, The University of Queensland, Brisbane, Australia.

[14] Kim, T. Y., Woo, J., Shin, D., and Kim, J., 1999, "Indirect Cutting Force Measurement in Multi-Axis Simultaneous NC Milling Processes," Int. J. Mach. Tools Manuf., **39**(11), pp. 1717–1731.

[15] Becker, R. S., Anderson, G. R., and Kovac, J., 1981, "An Investigation of the Mechanics and Noise Associated With Coal Cutting," ASME J. Eng. Ind., **103**(3), pp. 257–269.

[16] Idriss, O. S., Dimitrakopoulos, R., and Edwards, J. B., 1995, "The Effect of Orderly Vibration on Pickforce Sensing," Int. J. Surf. Min. Reclam. Environ., **9**(3), pp. 83–88.

[17] Krause, P. C., and Thomas, C. H., 1965, "Simulation of Symmetrical Induction Machinery," IEEE Trans. Power Apparatus Syst., **PAS-84**(11), pp. 1038–1053.

[18] Kelly, M., Hainsworth, D., Reid, D., Caris, C., and Gurgenci, H., 2005, "State of the Art in Longwall Automation," Longwall USA International Exhibition and Conference, Pittsburgh, PA, June 7–9.